JOURNAL OF MECHANICAL ENGINEERING AND SCIENCES
ISSN: 2289-4659 e-ISSN: 2231-8380
VOLUME 17, ISSUE 4, 2023, 9764 – 9777
DOI: https://doi.org/10.15282/jmes.17.4.2023.9.0773

UNIVERSITI MALAYSIA PAHANG AL-SULTAN ABDULLAH

RESEARCH ARTICLE

An adaptive model predictive control for coupled yaw and rollover stability of vehicle during corner maneuvers

A. Kumar[1], D.K. Dheer[2]*, and S. K. Verma[1]

[1] Department of Mechanical Engineering, National Institute of Technology Patna, Mahendru, Patna, 800005, Bihar, India
[2] Department of Electrical Engineering, National Institute of Technology Patna, Mahendru, Patna, 800005, Bihar, India
Phone: +91 6206398829

ABSTRACT - This paper presents a control strategy to achieve yaw and roll stability by taking into account the physical interaction between the yaw and roll dynamics to prevent vehicle collisions in hilly or curved terrain. The mathematical model is formulated utilizing a roll dynamic model with a small tyre slip angle and a bicycle model with two degrees of freedom considering coupling of yaw and roll dynamics. An adaptive model predictive controller and a PID controller are included in the proposed control methodology so that a real-time scenario of variation in the longitudinal velocity and friction coefficient is considered. Stability limits are established based on the yaw rate, sideslip, and roll motions of the vehicle, taking into account the effects of the road angle. The friction coefficients of 0.4 and 0.8 are chosen for wet and dry road surfaces to show manoeuvrability and force the vehicle to avoid rollover condition. Using numerical simulations in Matlab R2022a, the effectiveness of the designed controller is assessed. A root mean square error (RMSE) is calculated for the proposed methodology for the evaluation of the performance and the values are obtained as 3.032 and 3.912 for friction coefficient of 0.8 for yaw rate and roll angle respectively. On comparing with the other methodology, it is found that the performance of the proposed method is better based on RMSE. Also, the fluctuations at the corners are removed and the variables are bound inside the stability limit, thus avoiding the vehicle from accidents in hilly areas. The robustness of the controller towards increasing the mass of the vehicle by 5% and 10% is found to be good.

ARTICLE HISTORY
Received : 10th Apr. 2023
Revised : 06th Oct. 2023
Accepted : 26th Oct. 2023
Published : 26th Dec. 2023

KEYWORDS
Adaptive MPC
Lateral dynamics
Longitudinal dynamics
Yaw and roll
Vehicle stability
PID control

1.0 INTRODUCTION

To include the cutting-edge control techniques for safety and a high level of comfort in the automotive industry, several strategies, including active suspension systems, yaw stability, rollover prevention, active steering, and active braking systems are incorporated. These safety systems are developed to improve the stability, and handling of the vehicle. The accurate vehicle mathematical model is the requisite for developing and well performing of these systems. The model itself has developed from the simplified version to a coupling of the stability matrices. Different controllers are developed for these active safety systems, including sliding mode control, backstepping control, fuzzy control, and PID control [1].

Recently researchers have stressed the need for vehicles' roll stability systems to work in tandem with the handling systems i.e., lateral stability. Since the lateral dynamics and roll dynamics of a vehicle are both affected by the road friction coefficient that changes based on the dry and wet conditions. The risk of lateral instability, rather than rollover, is greater on low friction surfaces. However, increasing the road friction increases the chance of vehicle roll-over in comparison to lateral instability. On an icy road, the friction coefficient between the tires and road decreases even at low steering inputs, authors in [2] proposed a control technique to mitigate the yaw instability of the vehicles while steering. To improve the yaw stability of the vehicle, authors in [3, 4] developed a direct yaw control (DYC) and an integration approach of DYC and active front steering (AFS). Authors in [5], designed a dual model predicitive control (MPC) to handle the situations for both linear and saturation region of tire lateral force to improve yaw stability. To improve the yaw and roll stability, different approaches are available in the literature including developing of a priority based MPC for different steering including Fishhook and Double Lane Change (DLC) Maneuver [6], for differential braking and front/rear torque shifting is done for different road frictions [7], an integrated ESC system is applied instead of priority basis [8]. A new control algorithm combines differential braking and active suspension utilizing a fuzzy based PID is used to design a yaw and roll control system [9]. A similar control system is designed in [10], an active rear steering and direct yaw moment (ARS-DYC) coordination is developed based on a nonlinear fuzzy observation. For the yaw and roll stability of buses, a combined AFS, DYC, and Active Roll Moment (ARM) is implemented based on mixed H_2/H_∞ in [11]. For the different dynamics stability and control simultaneously, including yaw stability, roll stability, roll-yaw stability, and rollover prevention, a coordinated control strategy by toggling between different control modes [12]. An integrated control approach for yaw and roll over stability is proposed based on the differential braking [13]. The AFS and differential braking control are implemented for the yaw and rollover stability [14].

*CORRESPONDING AUTHOR | D.K. Dheer | ✉ dkdheer@nitp.ac.in

Due to the adaptability of MPC towards multi-variable constrained systems, model predictive control (MPC) has emerged as a promising approach in the field of unmanned systems for yaw and roll stability [15]. However, AGVs (Autonomous Ground Vehicles) can predict future events and adjust their actions accordingly. Therefore, it is natural to apply MPC algorithms to AGVs, given the characteristics of MPC and the needs of AGVs [16, 17]. An adaptive MPC is designed for a high center of mass in commercial vehicles for roll over stability prevention by considering inner wheel lifting condition [18]. With a model predictive control algorithm, authors in [19] proposed an adaptive path tracking control strategy for synchronizing active front wheel steering with the direct yaw moment for improving the path tracking ability under high speed and curvature. Based on the adaptive model following controller (AMFC) theory, a novel MIMO (multi-input-multi-output) controller is proposed to enhance the steering and roll stability of heavy vehicles considering lateral, yaw, and roll motion [20]. The work on tuning the weights of MPC are also done for better lateral and roll stability utilizing an extended bicycle model with a linear tire model with the help of evolutionary algorithms [21]. An extended MPC with differential evolution optimization algorithm is proposed to achieve lateral and roll dynamics [22]

Other than MPC, Electronic Stability Control (ESC) and steer by wire method [23], wireless control system [24] are employed to improve the yaw stability. Authors in [25], designed an artificial neural network controller for the shock absorbers to decrease the impact of vibration on patient's body by decreasing the damping coefficient. The active suspension of the trucks is developed with help of Deep Learning based Particle Swarm Optimization (DMPSO) to ease the driving comfort for the drivers[26]. During driving the heavy trucks, it is necessary for the driver to have a better nonlinear active suspension system, therefore authors in [27, 28] designed a robust artificial neural network controller to enhance the comfort and performance. The authors in [29], have included the rear steering angle of a 4WDIS during steady-state cornering (SSC), that show vehicle can perform SSC by increasing the yaw rate at high-speed using the opposite steering mode.

During the cornering maneuvers in the hill areas or curve on roads, the yaw rate may go beyond the stability limit due to improper brake force or steering input. Then the vehicle can spin around vertical axis and goes off the reference yaw rate. It may possible that due to high longitudinal velocity at the corners, the body of vehicle experiences a lateral acceleration beyond the limit and results in a rollover of the vehicle. In both the cases, the vehicle goes beyond the stability limit and leads to the accidents. Therefore, the objective of the research is to achieve the yaw stability and rollover prevention while considering the interaction while developing the mathematical model during cornering maneuver to avoid accidents. Practical scenarios are created with the help of simulation in Matlab by realizing the real cornering maneuvers by utilizing J turn and Fishhook maneuver. The different road conditions of wet and dry surface are considered by different friction coefficients and different longitudinal velocity. The yaw stability and rollover prevention safety systems helps the driver to avoid the vehicle from going outside the defined trajectory and to avoid the accidents during the cornering maneuver by bounding the variables inside the stability limit. These systems play an important role to control the vehicle in different dynamical motions. The yaw stability of the vehicle refers to the bounding of the yaw rate inside the defined stable boundary for different steering input and braking forces to avoid the spinning of vehicle around vertical axis. The rollover action is described as the lifting of the inner wheels while cornering leads to the rollover of the vehicle and thus leaves the defined trajectory.

In the literature, a tremendous work is done for yaw and rollover stability control system of the car like vehicle. The full car model is converted into a bicycle model based on assumptions that the tire slip angles of the front two and rear two tires are approximately same. The linear and nonlinear mathematical model of the vehicle is developed based on physics laws, but it is found that the coupling effect between yaw and roll dynamics is neglected, giving rise to a simplified model. Due to this, the information of the physical interactions between the two dynamical variables (yaw rate and roll angle) during cornering maneuver is lost and therefore the accuracy of a controller is not reliable. During the cornering, the longitudinal velocity and friction coefficient have a large implication on the yaw rate and roll dynamics, and their interactions. Still the literature lacks the exploring of the effect of selecting and analyzing different values of the two parameters. Therefore, authors find that the variation in the parameters has a large scope for achieving stability during cornering. To fulfil the objectives, the contributions made by the authors is that the physical interactions during cornering are incorporated i.e., coupling between yaw rate and roll dynamics are considered resulting in a complex model, however, it provides more realistic information. A PID controller is designed for longitudinal dynamics to decrease the longitudinal velocity up to a certain limit calculated based on vehicle parameters to avoid the rollover condition during the cornering maneuver. As the variation in the longitudinal velocity is considered, therefore an adaptive MPC (AMPC) is designed to incorporate these variations and to handle constraints applied on yaw dynamics to achieve yaw stability and a rollover situation is avoided.

2.0 MATHEMATICAL MODELLING

This paper focuses on developing a dynamic bicycle model for the vehicle to evaluate the proposed control strategy by exploiting the different critical driving maneuvers. To develop the model, the front two and rear two tires are assumed to show similar behavior, and therefore are lumped. In this section, a realistic model is developed by considering the coupling between the lateral and roll dynamics of the vehicle during curvature tracking according to Newton's laws of motion. The mathematical model is adopted from [21, 30–32] comprising lateral, yaw, and roll dynamics. The longitudinal velocity is allowed to follow a set point inside the defined range instead of assuming it to be a constant value. The bicycle model representing the lateral dynamics is shown in Figure 1.

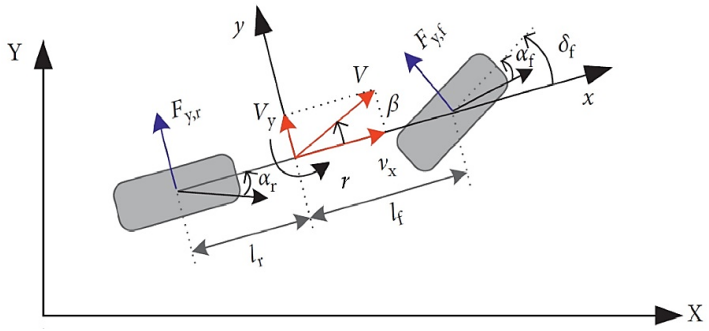

Figure 1. Bicycle model for lateral motion

The equation of motion for different dynamics are expressed here as:

Eq. (1) represents the lateral motion of vehicle with $\beta = tan^{-1}(v_y/V_x)$ as state variable:

$$mV_x(\dot{\beta} + r) + mh_r\dot{p} = F_{yf} + F_{yr} \tag{1}$$

The yaw motion of vehicle with respect to perpendicular axis (z) is given by Eq. (2):

$$I_z\dot{r} - I_{xz}\dot{p} = l_f F_{yf} - l_r F_{yr} \tag{2}$$

The roll motion with respect to longitudinal axis x is described by Eqs. (3) - (4):

$$\dot{\varphi} = p \tag{3}$$

$$(I_x + mh_r^2)\dot{p} - I_{xz}\dot{r} = -mh_r a_y - b_s\dot{\varphi} - k_s\varphi + mgh_r\varphi \tag{4}$$

where, m represents the mass of vehicle, V_x is the longitudinal velocity, β is the vehicle sideslip angle, r is the yaw rate, h_r is the height of center of gravity (CG), F_{yf} is the front tire lateral force, F_{yf} is the rear tire lateral force. The yaw moment of inertia is denoted by I_z, roll yaw moment of inertia is denoted by I_{xz}, roll moment of inertia is denoted by I_x. l_f is the distance of front axle from CG, l_r is the distance of rear axle from CG. The roll angle and roll rate are represented by φ and $\dot{\varphi}$ respectively. b_s and k_s are damping coefficient and roll stiffness coefficient of suspension. a_y and g are lateral acceleration and acceleration due to gravity respectively. The lateral acceleration of vehicle during cornering is defined by Eq. (5) as:

$$a_y = V_x\dot{\beta} + V_x r \tag{5}$$

The lateral forces [8] are approximated as linear functions for small tire slip angles. The front and rear tire lateral forces are calculated from Eqs. (6) – (7) as:

$$F_{yf} = C_f\alpha_f \tag{6}$$

$$F_{yf} = C_f\alpha_f \tag{7}$$

The front and rear tire slip angles are obtained from Eqs. (8) – (9) as:

$$\alpha_f = \delta - \beta - \frac{l_f r}{V_x} \tag{8}$$

$$\alpha_r = -\beta + \frac{l_r r}{V_x} \tag{9}$$

where, δ is the steering angle input, C_f and C_r are the linearized cornering stiffness of front and rear tires respectively. Table 1 represents the vehicle parameters required for developing the vehicle mathematical model.

Table 1. Vehicle parameters

Vehicle Simulation Parameters	Values
Mass, m	2449 kg
Distance of CG from Front Axle, l_f	1.547 m
Distance of CG from Rear Axle, l_r	1.217 m
Front Tire Cornering Stiffness, C_f	47000 N/rad
Rear Tire Cornering Stiffness, C_r	60000 N/rad

Table 1. (cont.)

Vehicle Simulation Parameters	Values
Height of CG, h_r	0.709 m
Yaw Moment of Inertia, I_z	4641 kgm^2
Roll Moment of Inertia, I_x	996 kgm^2
Roll Yaw Moment of Inertia, I_{xz}	187 kgm^2
Acceleration due to Gravity, g	9.8 ms^{-2}
Wheel Base, L	2.764 m
Track Width, l_s	1.5 m
Suspension Damping Coefficient, b_s	300 Nms/rad
Suspension Rolling Stiffness, k_s	23000 Nm/rad
Aerodynamic Drag, D_a	0.4
Road Inclination, θ	0.05 rad
Rolling Resistance, f_r	0.02

For the formulation of governing equations, let's assume that β, r, φ, and p as x_1, x_2, x_3, and x_4 respectively. Therefore, we obtain $[\dot{\beta}\ \dot{r}\ \dot{\varphi}\ \dot{p}]' = [\dot{x}_1\ \dot{x}_2\ \dot{x}_3\ \dot{x}_4]'$. Now assume,

$$\dot{x}_4 = x_5 \tag{10}$$

Using Eqs. (6) - (10) in Eqs. (1) - (2), to obtain the following equations:

$$\dot{x}_1 = \left(\frac{C_f}{mV_x}\right)\delta + x_1\left(\frac{-C_f - C_r}{mV_x}\right) + x_2\left(\frac{C_r l_r - C_f l_f - mV_x^2}{mV_x^2}\right) + x_5\left(\frac{-h_r r}{V_x}\right) \tag{11}$$

$$\dot{x}_2 = \left(\frac{l_f C_f}{I_z}\right)\delta + x_1\left(\frac{-l_f C_f + l_r C_r}{I_z}\right) + x_2\left(\frac{-l_r^2 C_r - l_f^2 C_f}{I_z V_x}\right) + x_5\left(\frac{I_{xz}}{I_z}\right) \tag{12}$$

On simplification, we obtained the equation defined as:

$$\dot{x}_4 = \left(\frac{(-h_r C_f I_z + l_f C_f I_{xz})}{(I_x I_z - I_{xz}^2)}\right)\delta + \left(\frac{(C_f + C_r)h_r I_z + (C_f l_f + C_r l_r)I_{xz}}{(I_x I_z - I_{xz}^2)}\right)x_1 + \left(\frac{(C_r l_r - C_f l_f - mV_x^2)(-h_r)}{V_x} + \frac{(-l_f^2 C_f - l_r^2 C_r)I_{xz}}{I_z V_x} - mh_r V_x\right)\left(\frac{I_z}{I_x I_z - I_{xz}^2}\right)x_2 + \left(\frac{(mgh_r - k_s)I_z}{(I_x I_z - I_{xz}^2)}\right)x_3 + \left(\frac{-b_s I_z}{(I_x I_z - I_{xz}^2)}\right)x_4 \tag{13}$$

Assuming the coefficients with δ, x_1, x_2, x_3, and x_4 as R_δ, R_1, R_2, R_3 and R_4 in the above Eq. (13). Substituting the value of $\dot{x}_4$ from Eq. (13) into Eqs. (11) – (12), we obtain:

$$\dot{x}_1 = \left(\frac{C_f}{mV_x} - \frac{h_r R_\delta}{V_x}\right)\delta + x_1\left(\frac{-C_f - C_r}{mV_x} - \frac{h_r R_1}{V_x}\right) + x_2\left(\frac{C_r l_r - C_f l_f - mV_x^2}{mV_x^2} - \frac{h_r R_2}{V_x}\right) + x_3\left(-\frac{h_r R_3}{V_x}\right) + x_4\left(-\frac{h_r R_4}{V_x}\right) \tag{14}$$

$$\dot{x}_2 = \left(\frac{l_f C_f}{I_z} + \frac{I_{xz} R_\delta}{I_z}\right)\delta + x_1\left(\frac{-l_f C_f + l_r C_r}{I_z} + \frac{I_{xz} R_1}{I_z}\right) + x_2\left(\frac{-l_r^2 C_r - l_f^2 C_f}{I_z V_x} + \frac{I_{xz} R_2}{I_z}\right) + x_3\left(\frac{I_{xz} R_3}{I_z}\right) + x_4\left(\frac{I_{xz} R_4}{I_z}\right) \tag{15}$$

Assuming the coefficients with δ, x_1, x_2, x_3, and x_4 in Eqs. (13), (14) as B_δ, B_1, B_2, B_3, B_4 and Y_δ, Y_1, Y_2, Y_3, Y_4. These coefficients vary in nature due to the longitudinal velocity. The state space representation is obtained by utilizing Eqs. (3), (13), (14), (15) defined by Eqs. (16) – (19) as:

$$\begin{bmatrix}\dot{x}_1\\ \dot{x}_2\\ \dot{x}_3\\ \dot{x}_4\end{bmatrix} = \begin{bmatrix}B_1 & B_2 & B_3 & B_4\\ Y_1 & Y_2 & Y_3 & Y_4\\ 0 & 0 & 0 & 1\\ R_1 & R_2 & R_3 & R_4\end{bmatrix}\begin{bmatrix}x_1\\ x_2\\ x_3\\ x_4\end{bmatrix} + \begin{bmatrix}B_\delta\\ Y_\delta\\ 0\\ R_\delta\end{bmatrix}[\delta] \tag{16}$$

$$\dot{X}_c(t) = A_c X_c(t) + B_c u(t) \tag{17}$$

$$\begin{bmatrix} y_1 \\ y_2 \\ y_3 \\ y_4 \end{bmatrix} = \begin{bmatrix} 1 & 0 & 0 & 0 \\ 0 & 1 & 0 & 0 \\ 0 & 0 & 1 & 0 \\ 0 & 0 & 0 & 1 \end{bmatrix} \begin{bmatrix} x_1 \\ x_2 \\ x_3 \\ x_4 \end{bmatrix} \tag{18}$$

$$Y_c(t) = C_c X_c(t) \tag{19}$$

Eqs. (17) and (19) are the continuous state space model for the formulation of Model Predictive Controller.

$$A_c = \begin{bmatrix} B_1 & B_2 & B_3 & B_4 \\ Y_1 & Y_2 & Y_3 & Y_4 \\ 0 & 0 & 0 & 1 \\ R_1 & R_2 & R_3 & R_4 \end{bmatrix}, B_c = \begin{bmatrix} B_\delta \\ Y_\delta \\ 0 \\ R_\delta \end{bmatrix} \tag{20}$$

This continuous model matrices in Eq. (20) are discretized into a discrete model required for the MPC [21]. For the discretization the Euler method is utilized as given below in Eq. (21):

$$A_d = e^{A_c T}, B_d = \int_0^T e^{A_c \tau} B_c d\tau \tag{21}$$

The discrete model thus obtained is represented as Eq. (22):

$$X_d(k+1) = A_d(k) X_d(k) + B_d(k) u(k) \tag{22}$$

$$Y_d(k) = C_d X_d(k) \tag{23}$$

Further, the augmented form of the model Eq. (22) for MPC is defined by Eqs. (24) – (25) as:

$$X_a(k+1) = A_a(k) X_a(k) + B_a(k) \Delta u(k) \tag{24}$$

$$Y_a(k) = C_a Y_a(k) \tag{25}$$

$$A_a(k) = \begin{bmatrix} A_d(k) & O_a^T \\ C_d A_d(k) & I_a \end{bmatrix}, B_a(k) = \begin{bmatrix} B_d(k) \\ C_d B_d(k) \end{bmatrix}, C_a = [O_a \quad I_a] \tag{26}$$

For the longitudinal dynamics of vehicle [26-28], the vehicle is decelerated by applying the braking force F_{xb} to achieve a longitudinal velocity V_x inside a defined range for the chosen maneuvers. The longitudinal motion during deceleration is defined by Eq. (27):

$$F_{xb} = -F_{xbf} - F_{xbr} - D_a - w\sin(\theta) \tag{27}$$

$$ma_x = -F_{xbf} - F_{xbr} - D_a - w\sin(\theta) \tag{28}$$

$$\dot{V}_x = \frac{-F_{xbf} - F_{xbr} - D_a - w\sin(\theta)}{m} \tag{29}$$

where, F_{xbf}, F_{xbr} are the front and rear braking force respectively. D_a is the aerodynamic drag, θ is the inclination angle of road, $w = mg$ is the normal load. During braking, the braking coefficient plays a vital role to distribute the total braking force between the front and rear tires.

This limits the deceleration to be approximately equal at both axles to avoid the directional stability and control. The braking coefficient is calculated in Eq. (30) as:

$$\frac{K_{bf}}{K_{br}} = \frac{\frac{l_r + h_r(\mu + f_r)}{L}}{\frac{l_f - h_r(\mu + f_r)}{L}} \tag{30}$$

where, K_{bf}, and K_{br} are the front and rear braking coefficient. For the K_{bf}, and K_{br}, the front and rear deceleration is calculated by Eqs. (31) – (32) defined as:

$$\left(\frac{d}{g}\right)_f = \frac{\frac{\mu l_r}{L} + K_{bf} f_r}{K_{bf} - \frac{\mu h_r}{L}} \tag{31}$$

$$\left(\frac{d}{g}\right)_r = \frac{\frac{\mu l_f}{L} + K_{br} f_r}{K_{br} + \frac{\mu h_r}{L}} \tag{32}$$

3.0 CONTROLLER DESIGN

The vehicle longitudinal and lateral motion control is achieved by designing the PID controller and adaptive MPC for two different steering input maneuvers. The objective of the longitudinal control design is to avoid the locking of either the front or rear tires earlier, thus preventing a loss of directional stability and control. To do this, the deceleration at both axles achieved by designing the PID control should be equal and given by Eq. (33) below:

$$\left(\frac{d}{g}\right)_f = \left(\frac{d}{g}\right)_r \tag{33}$$

The maximum allowable deceleration to the vehicle is obtained by Eqs. (31) and (32). The input to the vehicle is the front and rear brake force. During the braking, there is a longitudinal load transfer occurs limiting the maximum braking force at front and rear axle described the below Eqs. (34) and (35):

$$F_{bf,max} = \mu W_f = \frac{\mu W[l_r + h_r(\mu + f_r)]}{L} \tag{34}$$

$$F_{br,max} = \mu W_r = \frac{\mu W[l_f - h_r(\mu + f_r)]}{L} \tag{35}$$

The PID controller input and output is limited based on the physical limits. The controller gains k_p, k_i, and k_d is obtained after many trials and error method such that longitudinal velocity is decreased to the defined velocity range, time of travel and distance covered during deceleration. The time of travel t_b and distance covered B_d is defined in Eqs. (36) – (37) as:

$$t_b = \frac{V_{x,in} - V_{x,f}}{d} \tag{36}$$

$$B_d = \frac{V_{x,in}^2 - V_{x,f}^2}{2d} \tag{37}$$

The block diagram for controlled longitudinal dynamics is shown in Figure 2. The longitudinal motion is shown in the Figure 3 with help of mathematical blocks.

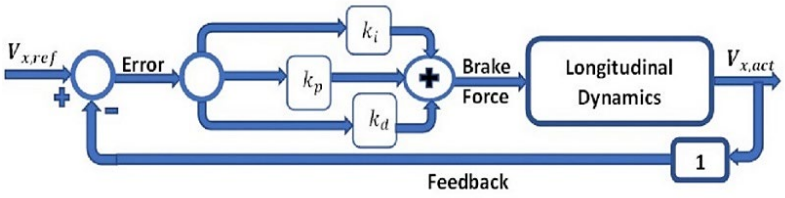

Figure 2. Block diagram for PID controller longitudinal dynamics

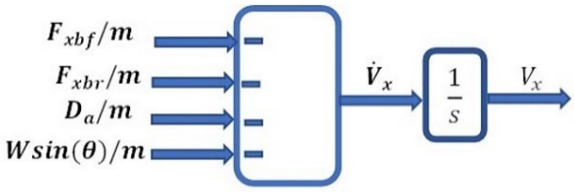

Figure 3. Block diagram of longitudinal motion

For the lateral motion control of the vehicle, adaptive MPC [33, 34] is designed due the variations in the longitudinal velocity. For the set point tracking of the varying parameter defined by the original discrete model Eqs. (22) and (23), the information of steady control input $u(k)$ is not possible. Therefore, the original model is modified to the incremented model defined in Eqs. (24) – (26) and are utilized to formulate the prediction model Eq. (38) for the adaptive MPC:

$$\hat{X}(k) = \hat{F}(k)X_a(k) + \hat{\phi}(k)\Delta U(k) \tag{38}$$

where,

$\hat{X}(k) = [\hat{x}(k+1|k)^T, \hat{x}(k+2|k)^T, \dots, \hat{x}(k+N_p|k)^T]^T$ and

$\Delta U(k) = [\Delta u(k)^T, \Delta u(k+1)^T, \dots, \Delta u(k+N_c-1)^T]^T$ and the predictive matrices are given by Eqs. (39) – (40) as:

$$\hat{F}(k) = \begin{bmatrix} A_a(k) \\ A_a^2(k) \\ . \\ . \\ . \\ A_a^{N_p}(k) \end{bmatrix} \tag{39}$$

$$\hat{\phi}(k) = \begin{bmatrix} B_a(k) & 0 & 0 & 0 & 0 & 0 \\ A_a(k)B_a(k) & B_a(k) & 0 & 0 & 0 & 0 \\ A_a^2(k)B_a(k) & A_a(k)B_a(k) & B_a(k) & 0 & 0 & 0 \\ . & . & . & . & 0 & 0 \\ . & . & . & . & . & 0 \\ A_a^{N_p-1}(k)B_a(k) & A_a^{N_p-2}(k)B_a(k) & A_a^{N_p-3}(k)B_a(k) & . & . & A_a^{N_p-N_c}(k)B_a(k) \end{bmatrix} \tag{40}$$

In each sampling interval, the AMPC solves a constrained optimization problem to obtain the optimal sequence of control input. The cost function of the AMPC for the system Eq. (24) is opted as defined by Eq. (41):

$$\min_{\Delta U} J(k) = \sum_{i=1}^{N_p} \left\| Q(k+i|k)(\hat{X}(k+i|k) - r) \right\|_2^2 + \sum_{i=0}^{N_c-1} \| R(k+i|k)(\Delta u(k+i|k)) \|_2^2 \tag{41}$$

where, $\|.\|_2^2$ is the square of Euclidean norm. N_p and N_c are the prediction and control horizon with $N_c \leq N_p$. Q and R are the weight matrices on the tracking errors and control input defined by Eq. (42):

$$Q = diag(W_\beta, W_r, W_\phi, W_{\dot{\phi}}) \tag{42a}$$

$$R = W_\delta \tag{42b}$$

The cost function is subjected to the state dynamics and physical linear constraints defined by Eq. (43) as:

$$\hat{X}_{min} \leq \hat{X}(k+i) \leq \hat{X}_{max} \tag{43a}$$

$$\Delta U_{min} \leq \Delta U \leq \Delta U_{max} \tag{43b}$$

To implement the AMPC, the reference values of states should be defined. The yaw rate is bounded by its maximum value considering the load transfer ratio (LTR) to prevent from roll-over. The reference yaw rate r_{ref} is described by Eq. (44):

$$r_{ref} = \min(|r_{ss}|, |r_{max,LTR}|) sign(\delta_f) \tag{44}$$

The steady state value r_{ss} and maximum value of yaw rate $r_{max,LTR}$ is obtained from Eqs. (45) – (46) as:

$$r_{ss} = \frac{LV_x\delta}{L^2 - 0.5mV_x^2\left(\frac{l_f}{C_r} - \frac{l_r}{C_f}\right)} \tag{45}$$

$$r_{max,LTR} = \frac{LTR_{th}l_s g}{2h_r V_x} \tag{46}$$

The reference sideslip angle β_{ref} is defined by Eq. (47) as:

$$\beta_{ref} = \min(|\beta_{ss}|, |\beta_{max}|) sign(\delta_f) \tag{47}$$

The steady state and maximum value of sideslip angle is described from Eqs. (48) – (49) as:

$$\beta_{ss} = \frac{l_r L - 0.5mV_x^2\left(\frac{l_f}{C_r}\right)}{L^2 - 0.5mV_x^2\left(\frac{l_f}{C_r} - \frac{l_r}{C_f}\right)}\delta \tag{48}$$

$$\beta_{max} = \arctan(0.02\mu g) \tag{49}$$

The reference value of ϕ and $\dot{\phi}$ are chosen to be zero ideally, as the vehicle body should not generate any roll motion but practically this is not possible during a cornering manoeuvring. The assumed threshold value of LTR for which simulation is done is 0.7, however, the stable region for avoiding a rollover condition is [-1,1] [31]. The LTR is obtained by Eq. (50):

$$LTR = \frac{2h_r a_y \cos(\phi)}{l_s g} + \frac{2h_r \sin\phi}{l_s} \tag{50}$$

The adaptive control law of the MPC is generated by incorporating the variations present in longitudinal velocity. The adaptive MPC controller revises the model of the plant and the setpoints at regular intervals. Once an update is made to the model and corresponding conditions, they will remain unchanged throughout the duration of the forecast. The updated discrete plant model and nominal operating conditions required by the adaptive MPC is defined by Eq. (51):

$$\begin{aligned} A_a(k+1) &= A_a(k) \\ B_a(k+1) &= B_a(k) \\ C_a(k+1) &= C_c(k) \\ x_a(k+1) &= x_a(k) \\ \Delta u(k+1) &= \Delta u(k) \\ y_a(k+1) &= y_a(k) \\ Dx_a(k+1) &= A_a(k)x(k) + B_a(k)\Delta u(k) - x(k) \end{aligned} \tag{51}$$

Every time step, the adaptive MPC uses Eq. (50) to update the plant model and the operating condition (states). From the plant model, we get the state values at the previous time step, and with the help of the parameters of interest fed into the model updating block, we can compute the augmented discrete variable system matrices $A_a(k)$, $B_a(k)$, and $C_a(k)$. Therefore, at each sampling interval, the AMPC's QP problem, Eq. (34), will be adapted to the most recent model, Eq. (38).

4.0 RESULTS AND DISCUSSION

In this work, a 3 DOF vehicle model is utilized with a tire model for the small slip tire angles during the lateral motion. The coupling between roll dynamics with lateral and yaw motion is considered for a better realization of dynamics. The PID controller is implemented for longitudinal motion, and an adaptive MPC is exploited for lateral and roll stability. For longitudinal motion, V_x is set as 120 km/h as initial velocity V_{in}. The friction coefficient μ is chosen to be 0.4 and 0.8 to represent wet and dry surface. Table 1 shows the obtained values of deceleration for different friction coefficient and braking coefficients for V_{in} = 120 km/h. From the table, it is observed that the calculated maximum deceleration for front and rear tires is equal. The simulation is performed in Matlab platform with a version of R2022a on the 11th Gen Intel(R) Core (TM) i5-1135G7 @ 2.40GHz processor.

Table 2. Calculated braking coefficient and maximum deceleration for $\boldsymbol{\mu}$ = 0.4, and 0.8

Friction Coefficient, μ	Braking Coefficient	Max deceleration
0.4	K_{bf} = 0.547	d_f = 0.42g
	K_{bf} = 0.452	d_r = 0.42g
0.8	K_{bf} = 0.650	d_f = 0.82g
	K_{bf} = 0.394	d_r = 0.82g

4.1 Simulation Results

To evaluate the proposed control strategy over the selected vehicle mathematical model, different control input maneuvers are available in the literature, including J - turn, fishhook, sine wave, and double lane change. In our analysis, the motive of the controller is to enforce the designed vehicle model to achieve directional stability and directional control during longitudinal motion on a straight path. And, during the curved trajectory, the vehicle should be bound inside the stability region for both, lateral and roll dynamics. In J-turn and fishhook maneuvers, the vehicle is allowed to follow a straight line, and brakes are applied to achieve a longitudinal velocity at the start of the curve trajectory for a stable operation. Therefore, J-turn and fishhook maneuvers are opted as control input steering angles.

4.2 J-Turn Maneuver

In this driving scenario, the vehicle is first decelerated up-to a certain longitudinal velocity in a specified range. The friction coefficient is taken as 0.4, 0.8 and initial longitudinal velocity of 120 km/h. The brake force is distributed among the front and rear tires to decrease the longitudinal velocity.

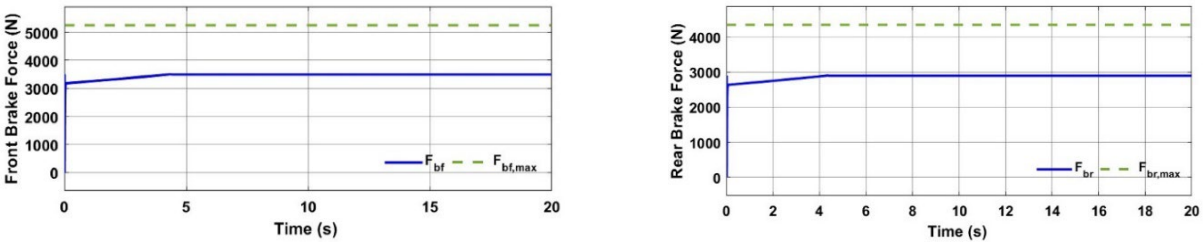

(a) (b)

Figure 4. Brake forces: (a) Front brake force and (b) Rear brake force

The brake forces obtained in simulation are observed to be below the maximum calculated brake force. For the time interval $0s \leq t \leq 4.3s$, the F_{xb} value increases to decrease the longitudinal velocity to 62 km/h. After the time $t \geq 4.3s$, the F_{xb} becomes constant to maintain the set value of V_x. Due to the longitudinal load transfer during braking, the front braking force is greater than the rear. The deceleration (in g) of both the front and rear tires is shown in Figure 5.

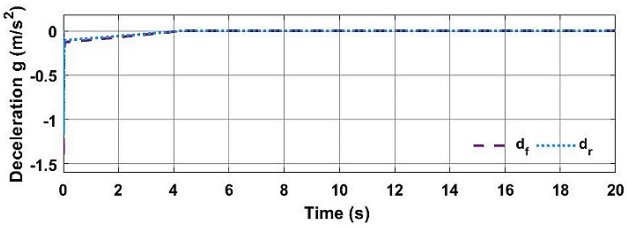

Figure 5. Front and rear tires deceleration (in g)

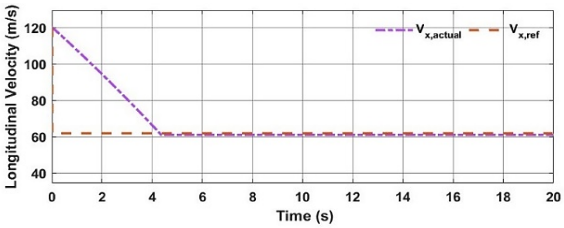

Figure 6. Longitudinal velocity of vehicle

From the figure, it is seen that the deceleration of both tires is approximately equal. The deceleration increases up to the time $t \leq 4.3\ s$ and after the time $t = 4.3\ s$, the $d_f = d_r = 0$. The longitudinal velocity of the vehicle is shown in Figure 6. The desired longitudinal velocity is achieved at the time $t = 4.3\ s$ due the application of brake force. During the lateral motion of the J – turn maneuver, the vehicle is operated around the set velocity, and variations in the state variables are obtained to analyze the performance of the adaptive controller. The sideslip angle during the J – turn maneuver is shown in Figure 7(a). From the figure, it is observed that the actual sideslip angle is inside the defined boundary and the slope that is being observed is due to physical constraints. Figure 7(b) depicts the yaw rate of the vehicle during the maneuver. It can be seen that the tracking of the reference yaw rate is within the boundary defined. The peak values for both the output variables are observed for the time interval $4.5\ s \leq t\ \leq 5.5\ s$.

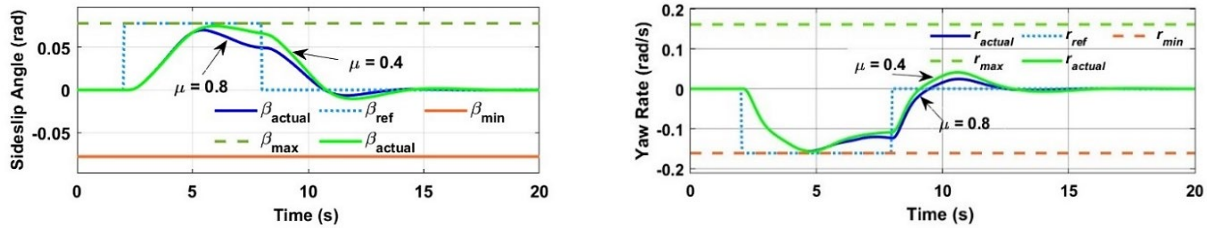

(a) (b)

Figure 7. J – turn maneuver: (a) Sideslip angle and (b) Yaw rate

The roll angle and roll rate are shown in Figures 8. The roll dynamics are observed to be inside the stability limit, thus generating the lateral load transfer ratio below the threshold value. The roll angle is at its peak value for the time interval $4s \leq t \leq 6s$. The lateral acceleration is shown in Figure 9. The lateral acceleration is observed to be below the maximum value obtained μg. The lateral acceleration is observed to be at its peak value for the time interval during which the yaw rate and side slip angle are the peak value observed at the corner. The LTR for both friction coefficients is shown in Figure 10. For the value of μ, the LTR has increased, and peaks are observed at high values of roll angle.

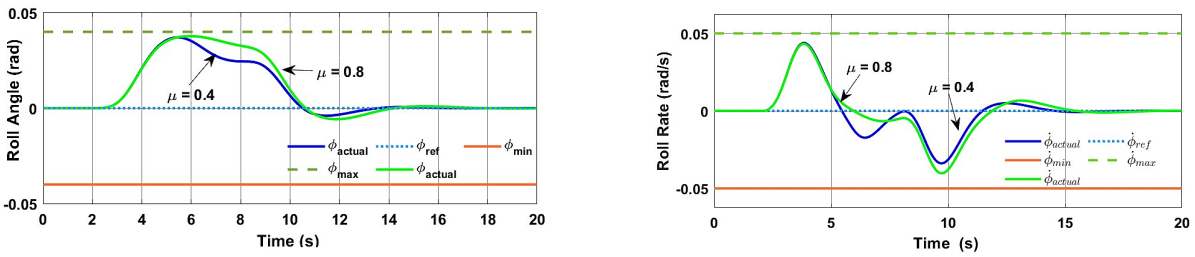

(a) (b)

Figure 8. J – turn maneuver: (a) Roll angle and (b) Roll rate

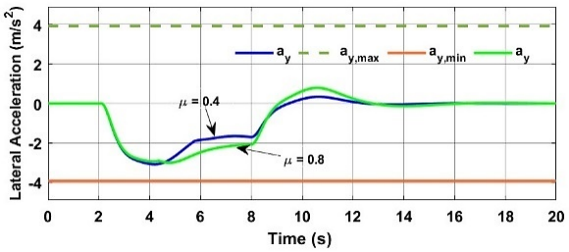

Figure 9. Lateral acceleration for J – turn maneuver

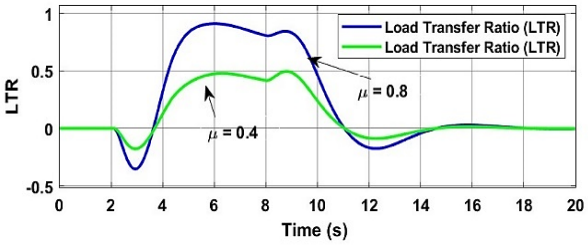

Figure 10. LTR for J – turn maneuver

4.3 Fishhook (FH) Maneuver

In this maneuver, the longitudinal velocity performs the same as of J – turn maneuver to bring down the velocity to 62 km/h. For lateral dynamics, the simulation is done for the analysis of output variables for the stability. Friction coefficients of $\mu = 0.4, 0.8$ are utilized to observe the controller performance. Figure 11(a) shows the sideslip angle for the fishhook maneuver. The tracking is observed to be within the stable region for both values of the friction coefficient. The peak value of the sideslip angle is observed at time interval $6s \leq t \leq 8s$. Figure 11(b) depicts the yaw rate tracking. The yaw rate is inside the limits defined. The peak value of the yaw rate is seen at time interval $5s \leq t \leq 7s$. The increasing and decreasing slopes of both output variables represent the limitation of the variation in the physical variables.

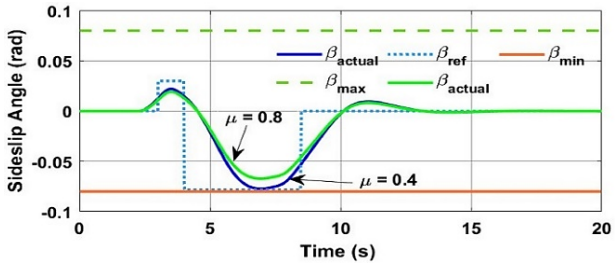

(a)

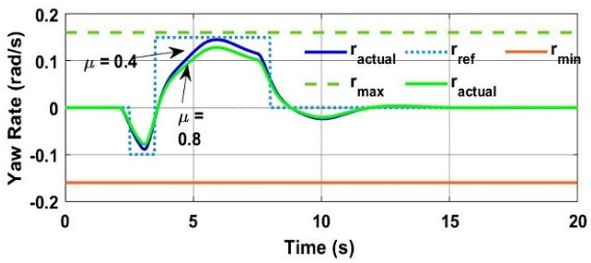

(b)

Figure 11. Fishhook maneuver: (a) Sideslip angle and (b) Yaw rate

The roll angle and roll rate for the fishhook maneuver are shown in Figure 12(a) and (b). The roll dynamics for the fishhook maneuver are seen to be bound within the stability limit. The peak value of roll angle for a lower friction coefficient is greater than that for a high value of μ. The peak occurs for the time interval $6s \leq t \leq 8s$. The lateral acceleration for the fishhook maneuver is shown in Figure 13 for wet and dry surfaces. The value of a_y experienced by the body of the vehicle attains the peak value for the time interval $6s \leq t \leq 8s$ generating the peak value of ϕ for the same time interval. The LTR for the fishhook maneuver is shown in Figure 14. The value of higher at high value of roll angle while cornering. As the value of the friction coefficient decreases, the value of LTR also decreases.

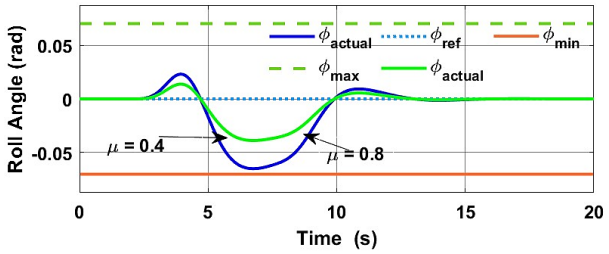

(a)

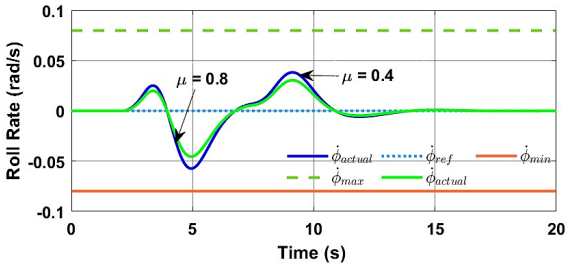

(b)

Figure 12. FH maneuver: (a) Roll angle and (b) Roll rate

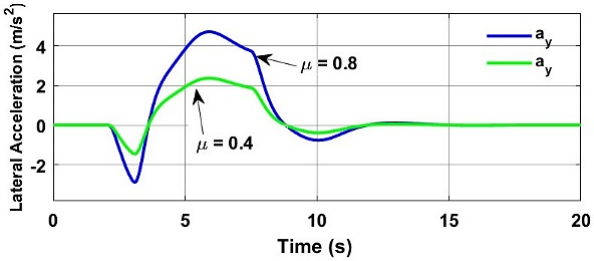

Figure 13. Lateral acceleration for FH maneuver

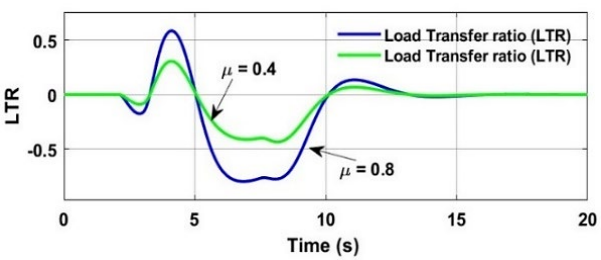

Figure 14. LTR for FH maneuver (LTR)

The proposed control methodology is compared with the previous state of the art [12-14] to show that the yaw and roll stability has improved in the obtained results. From the results obtained in [12], for the fishhook maneuver (FH), it is observed that the yaw rate and the roll angle comprise of fluctuations at the extreme peak values. Due to the presence of these transients, a smooth cornering is not obtained, and the vehicle is susceptible to noise. A similar result is obtained in [13] for the case of yaw rate. High peaks are obtained at the corners beyond the reference values for the yaw rate. Also, the transients are present with the error values. In [14], the yaw rate and roll angle obtained are deflected from the desired values. A lane change maneuver (LC) response for the proposed methodology is also compared with [12-14]. In [12], the yaw rate and roll angle comprise of the transients, affecting the performance of the vehicle. Similarly, in [14] , the presence of the fluctuations throughout the lane changing time interval reduces the stability of vehicle. In a braking and cornering scenario to decrease the longitudinal velocity, the small fluctuation may cause the vehicle to go into the region of instability and accident may occur.

Figures 15(a) and 15(b) depicts the obtained yaw rate and roll angle after implementing the methods in [12-14] for the fishhook maneuver. Figures 16(a) and 16(b) shows the yaw rate and roll angle for the lane change maneuver after applying the methods proposed in [12-14]. From the Figures for FH and LC maneuver, it is observed that, the transients and fluctuations are present. The adaptive control methodology of the model predictive control has removed these problems and minimized possibility of the vehicle to go outside the region of stability.

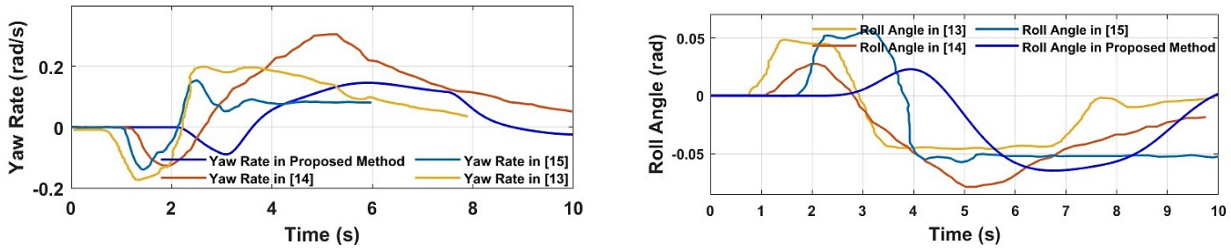

(a) (b)

Figure 15. FH comparison: (a) Yaw rate and (b) Roll angle

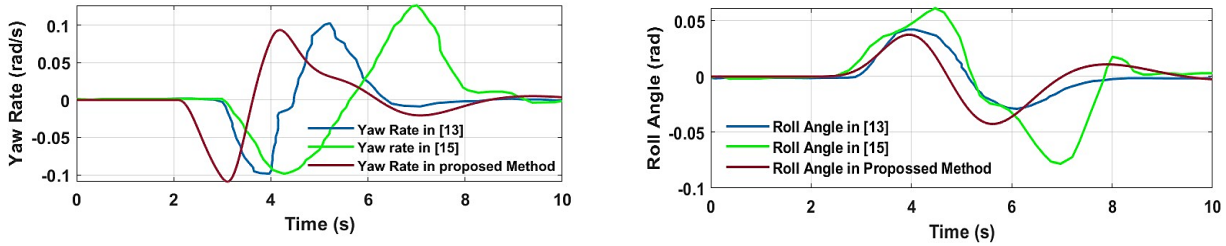

(a) (b)

Figure 16. LC comparison: (a) Yaw rate and (b) Roll angle

Further, the control methodology proposed is tested on the vehicle parameters of [13] for the comparison purpose with respect to fishhook maneuver. Figure 17(a) represents the yaw rate and Figure 17(b) depicts the roll angle. From these Figures it is evident that the control methodology has decreased the amount of error calculated by the RMSE.

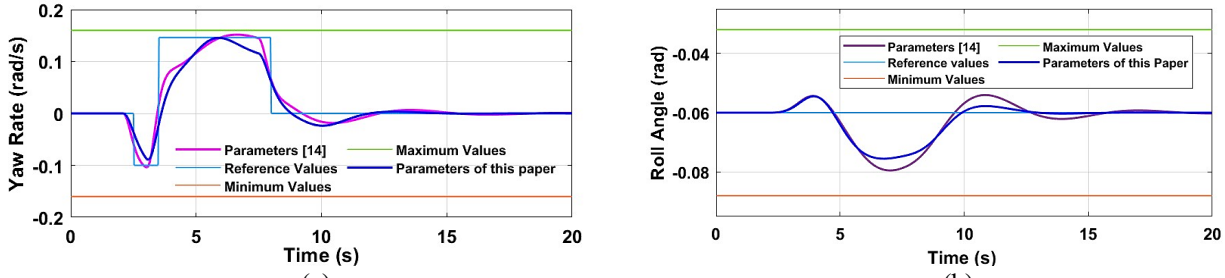

(a) (b)

Figure 17. Proposed method comparison with [14]: (a) Yaw rate (b) Roll angle

The RMSE values are obtained to compare the performance of the control methodology utilizing the Eq. (52).

$$\text{RMSE} = \sqrt{\text{mean}(R - Y)^2} \tag{52}$$

where, R is the reference values and Y is the actual values of the yaw rate. Table 3 show the comparison of RMSE values of the yaw rate obtained by the proposed method and the method in [14] for the fishhook maneuver as input steering angle.

Table 3. RMSE comparison of yaw rate for fishhook maneuver

State Variable	RMSE Values
Yaw Rate for proposed method ($\mu = 0.4$ and 0.8)	2.234 and 3.023 respectively
Yaw Rate [14]	4.7236

From the table, it is observed that the error values for the proposed method is less in comparison to [13]. The RMSE value is calculated based on Eq. (52) utilizing the parameters of [13] and the proposed control methodology. Table 4 shows the RMSE values for yaw rate and the roll angle. From the Table 4, it can be seen that the proposed methodology has decreased the error values obtained in [13].

Table 4. RMSE comparison for yaw rate and roll angle for fishhook maneuver

State Variable	Vehicle Parameter	RMSE Values
Yaw Rate	[13]	3.823
Roll Angle	[13]	4.534
Yaw Rate	Proposed Method	3.023
Roll Angle	Proposed Method	3.912

While implementing cornering maneuvers such as J-turn and fishhook maneuvers, the longitudinal velocity is decreased within a defined limit. Therefore, the PID controller decreases the velocity from 120 km/h to 62 km/h. Since, there is longitudinal load transfer during braking, the maximum values of the front and rear tires are 5300 N and 4300 N, obtained from calculation. The obtained values of front and rear brake forces from simulation are below the maximum value. The deceleration values obtained for both axles are approximately equal, with a peak starting when the force is applied. The value of deceleration obtained from simulation is 0.25 g, which is below the maximum value of 0.42 g.

The yaw and roll dynamics obtained from simulation show stable performance. The peak values of all the sideslip angle, yaw rate, and roll angle occur at the same time interval for both input maneuvers. The values of sideslip angle and yaw rate obtained for a friction coefficient of 0.4 (wet road) are higher as compared to the values for a friction coefficient of 0.8 (dry road). This is due to the fact that the lateral tire force diminishes on the wet surface and increases on the dry surface due to the high friction of the road. The roll angle is higher for a higher friction coefficient as the lateral acceleration experienced by the body of the vehicle is greater than that of a lower friction coefficient value. Due to the higher roll angle of the dry road surface the value of LTR increases as compared to the wet surface road. The value of LTR lies inside the stable region [-1,1] for both types of roads, representing that the vehicle is prevented from rolling. The range of validity for the obtained results for different maneuvers are based on the stability region of the vehicle. The stable region of vehicle operation is bounded by the maximum and minimum values of the yaw rate and LTR. The stable region of the yaw stability considering the influence of the roll angle is obtained by utilizing the vehicle parameters and the longitudinal velocity. The roll stability is also obtained by considering the LTR formula comprising of lateral acceleration, roll angle, and vehicle parameters. The yaw rate and the side slip angle are the direction function of input steering angle. The value of the steering angle is a physical constraint. For the obtained results, the range of steering angle for the operation is considered as ± 0.3 rad.

The proposed method for obtaining yaw and roll stability is compared with the other methodology available, further, the proposed control methodology is applied on the other vehicle model for the validity of the obtained results. The results obtained in the proposed methodology of our research, the transients and the steady state error values are minimized and removed respectively. To verify the robustness of the controller, the mass of the vehicle is increased by 5% and 10%, the friction coefficient is kept at $\mu = 0.8$, and the simulation conditions are same for the fishhook maneuver. Figures 18(a) & 18(b) shows the robustness simulation results of the control methodology when the vehicle mass changes. From the figures, it is evident that the effect of mass change on the yaw rate and the roll angle has a little change, and the control system is able to maintain a good control effect.

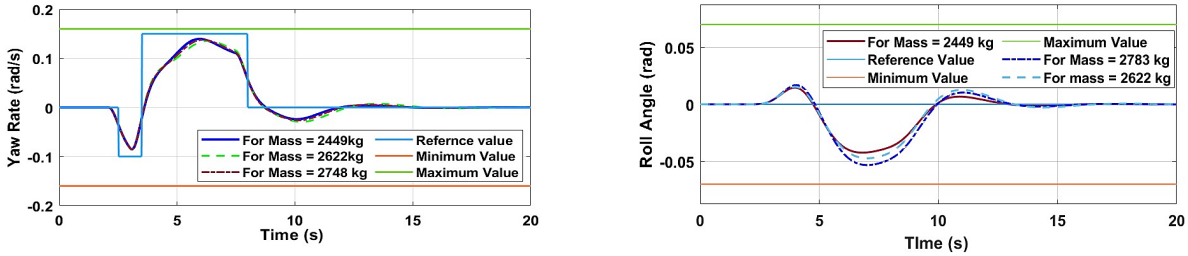

(a) (b)

Figure 18. Robustness for different masses: (a) Yaw rate change and (b) Roll angle change

5.0 CONCLUSION

In this paper, an adaptive model predictive controller is designed to include the physical interactions between the yaw and roll dynamics, while considering the longitudinal velocity to be decreasing. A PID controller is designed for controlling the longitudinal velocity on a road with an inclination. The proposed control approach is simulated for wet and dry road surfaces to show the performance of the controller for different road frictions. Inputs are chosen as, J-turn and fishhook maneuvers due to their versatile nature. The stability matrices, such as yaw rate and roll angle, are obtained inside the boundary limits defined with the help of vehicle parameters for both types of road surface. The value of LTR obtained is inside the assumed threshold value, preventing the vehicle from rolling over. The simulation results show that the proposed methodology has improved yaw and rollover stability. A RMSE value of 3.032 and 3.912 for friction coefficient of 0.8 is calculated for the proposed methodology for yaw rate and roll angle respectively. Further, the control methodology is applied on different vehicle parameter and found a decrease in RMSE value from 4.7236 to 3.823. The RMSE calculated shows that the control method has performed well. The robustness of the controller is found to be good after implementing an increase in the mass of the vehicle by 5% and 10% in the simulation. Due to interactions considered in this paper, the tracking of reference values for sideslip angle and yaw rate comprises of slopes. Therefore, the future scope of the paper is to improve further tracking of reference values with the non-linear vehicle model.

6.0 ACKNOWLEDGMENTS

The authors would like to acknowledge National Institute of Technology Patna, India for providing the platform for the research.

7.0 REFERENCES

[1] H. Termous, H. Shraim, R. Talj, C. Francis, and A. Charara, "Coordinated control strategies for active steering, differential braking and active suspension for vehicle stability, handling and safety improvement," *Vehicle System Dynamics*, vol. 57, no. 10, pp. 1494–1529, 2019.

[2] Y. Zhu, H. Li, K. Wang, Y. Bao, and P. Zeng, "A simulation study for lateral stability control of vehicles on icy asphalt pavement," *Journal of Advanced Transportation*, vol. 2022, p. 7361881, 2022.

[3] Y. Song, H. Shu, X. Chen, and S. Luo, "Direct-yaw-moment control of four-wheel-drive electrical vehicle based on lateral tyre-road forces and sideslip angle observer," *IET Intelligent Transport Systems*, vol. 13, no. 2, pp. 356–366, 2019.

[4] N. Ahmadian, A. Khosravi, and P. Sarhadi, "Driver assistant yaw stability control via integration of AFS and DYC," *Vehicle System Dynamics*, vol. 60, no. 5, pp. 1742–1762, 2022.

[5] S. Li, G. Wang, B. Zhang, Z. Yu, and G. Cui, "Vehicle yaw stability control at the handling limits based on model predictive control," *International Journal of Automotive Technology*, vol. 21, no. 2, pp. 361–370, 2020.

[6] L. Li, Y. Lu, R. Wang, and J. Chen, "A three-dimensional dynamics control framework of vehicle lateral stability and rollover prevention via active braking with MPC," *IEEE Transactions on Industrial Electronics*, vol. 64, no. 4, pp. 3389–3401, 2017.

[7] R. Hajiloo, A. Khajepour, A. Kasaiezadeh, S. K. Chen, and B. Litkouhi, "Integrated lateral and roll stability control of multi-actuated vehicles using prioritization model predictive control," *IEEE Transactions Vehicular Technology*, vol. 71, no. 8, pp. 8318–8329, 2022.

[8] J. Ji, A. Khajepour, W. W. Melek, and Y. Huang, "Path planning and tracking for vehicle collision avoidance based on model predictive control with multiconstraints," *IEEE Transactions on Vehicular Technology*, vol. 66, no. 2, pp. 952–964, 2017.

[9] H. Li, Y. Zhao, F. Lin, and H. Xu, "Integrated yaw and rollover stability control of an offroad vehicle with mechanical elastic wheel," *Journal of Vibroengineering*, vol. 21, no. 2, pp. 450–471, 2019.

[10] C. Sun, Z. Xu, B. Tong, S. Deng, "Integration sliding mode control for vehicle yaw and rollover stability based on nonlinear observation," *Transactions of the Institute of Measurement and Control*, vol. 44, no. 15, pp. 3039–3056, 2022.

[11] X. Li, X. Lu, H. Zhang, "Tracking control for rollover prevention and yaw stability for commercial buses," Institute of Electrical and Electronics Engineers, *IEEE 16th International Conference on Control & Automation (ICCA), country* pp. 1193-1198, 2020.

[12] T. Xu, X. Wang, C. Ma, X. Wei, "Coordinated control strategy of roll-yaw stability and path tracking for centralized drive electric vehicles," *Proceedings of the Institution of Mechanical Engineers, Part D: Journal of Automobile Engineering*, vol. 237, no. 6, pp. 1260–1276, 2022.

[13] H. Q. Li, Y. Q. Zhao, F. Lin, Z. Xiao, "Integrated yaw and rollover control based on differential braking for off-road vehicles with mechanical elastic wheel," *Journal of Central South University*, vol. 26, no. 9, pp. 2354–2367, 2019.

[14] H. Zheng, Y. Miao, B. Li, "Comparison of active front wheel steering and differential braking for yaw/roll stability enhancement of a coach," *SAE International Journal of Vehicle Dynamics Stability and NVH*, vol. 2, no. 4, pp. 267–283, 2018.

[15] M. Ataei, A. Khajepour, and S. Jeon, "Model predictive control for integrated lateral stability, traction/braking control, and rollover prevention of electric vehicles," *Vehicle System Dynamics*, vol. 58, no. 1, pp. 49–73, 2020.

[16] M. A. Kamel, A. T. Hafez, X. Yu, "A review on motion control of unmanned ground and aerial vehicles based on model predictive control techniques," *Engineering Science and Military Technologies*, vol. 2, no. 1, pp. 10-23, 2018.

[17] S. Yu, M. Hirche, Y. Huang, H. Chen, F. Allgöwer, "Model predictive control for autonomous ground vehicles: A review," *Autonomous Intelligent Systems*, vol. 1, no. 4, pp. 1-17, 2021.

[18] C. Zhou, L. Yu, Y. Li, Z. Lu, J. Song, "A layered roll stability control strategy for commercial vehicles based on adaptive model predictive control," *Vehicle System Dynamics*, vol. 61, no. 12, pp. 3067-3088, 2022.

[19] Y. Tian, Q. Yao, P. Hang, S. Wang, "Adaptive coordinated path tracking control strategy for autonomous vehicles with direct yaw moment control," *Chinese Journal of Mechanical Engineering*, vol. 35, no. 1, pp. 1-15, 2022.

[20] Y. Lu, J. Zhang, H. Li, Y. Han, "A novel adaptive model following controller to enhance steering and roll stability of heavy vehicle," *Journal of Mechanical Science and Technology*, vol. 35, no. 12, pp. 5287–5297, 2021.

[21] R. Prakash, D. K. Dheer, "Evolutionary algorithms-based model predictive control for vehicle lateral and roll motion control," *Arabian Journal for Science and Engineering*, vol. 48, no. 5, pp. 6857–6871, 2023.

[22] Q. Liu, S. Song, H. Hu, T. Huang, "Extended model predictive control scheme for smooth path following of autonomous vehicles," *Frontiers of Mechanical Engineering*, vol. 17, no. 1, pp. 1-16, 2022.

[23] R. Rajamani, D. N. Piyabongkarn, "New paradigms for the integration of yaw stability and rollover prevention functions in vehicle stability control," *IEEE Transactions on Intelligent Transportation Systems*, vol. 14, no. 1, pp. 249–261, 2013.

[24] M. S. M. Aras, M. K. M. Zambri, F. A. Azis, M. Z. A. Rashid, M. N. Kamarudin, "System identification modelling based on modification of all terrain vehicle (ATV) using wireless control system," *Journal of Mechanical Engineering and Sciences*, vol. 9, pp. 1640–1654, 2015.

[25] A. Hamza, N. Ben Yahia, "Artificial neural networks controller of active suspension for ambulance based on ISO standards," *Proceedings of the Institution of Mechanical Engineers, Part D: Journal of Automobile Engineering*, vol. 237, no. 1, pp. 34–47, 2023.

[26] A. Hamza, N. B. Yahia, "Deep learning based intelligent active suspension control for heavy trucks (DMPSO)," *Advances in Mechanical Engineering and Mechanics II*: *Lecture Notes in Mechanical Engineering*, 2022, pp. 347–354.

[27] A. Hamza, N. Ben Yahia, "Heavy trucks with intelligent control of active suspension based on artificial neural networks," *Proceedings of the Institution of Mechanical Engineers. Part I: Journal of Systems and Control Engineering*, vol. 235, no. 6, pp. 952–969, 2021.

[28] A. Hamza and N. Ben Yahia, "Intelligent neural network control for active heavy truck suspension," *Advances in Mechanical Engineering and Mechanics: Lecture Notes in Mechanical Engineering*, 2019, pp. 16–23.

[29] M. Li, M.I. Ishak, P.M. Heerwan, "A numerical simulation of vehicle dynamics behavior for a four-wheel steering vehicle with the passive control system," *Journal of Mechanical Engineering and Sciences*, vol. 16, no. 2, pp. 8953–8964, 2022.

[30] J. Y. Wong, Theory of Ground Vehicles, 3rd Ed. *John Wiley*, New York, United States, 2001.

[31] T. D. Gillespie, Fundamentals of Vehicle Dynamics, Revised Ed. *Society of Automotive Engineers International*, Pennsylvania, United States, 2021.

[32] R. Rajamani, Vehicle Dynamics and Control, 2nd Ed. *Springer*, United States, 2012.

[33] A. Dhar and S. Bhasin, "Adaptive MPC for uncertain discrete-time LTI MIMO systems with incremental input constraints," *International Federation of Automatic Control*, vol. 51, no 1, pp. 329–334, 2018

[34] C. Jia, W. Qiao, J. Cui, L. Qu, "Adaptive model-predictive-control-based real-time energy management of fuel cell hybrid electric vehicles," *IEEE Transactions on Power Electronics*, vol. 38, no. 2, pp. 2681–2694, 2023.